Thermodynamic Stability of Heterodimetallic [LnLn'] Complexes: Synthesis and DFT Studies

Joan Gónzalez-Fabra,[a] Nuno A. G. Bandeira,[a][b][c] Verónica Velasco,[d] Leoní A. Barrios,[d] David Aguilà,[d] Simon J. Teat,[e] Olivier Roubeau,[f] Carles Bo*[a][g] and Guillem Aromí*[d]

[a] Mr J. Gónzalez-Fabra, Dr. N. A. G. Bandeira, Dr C. Bo
Institute of Chemical Research of Catalonia (ICIQ), The Barcelona Institute of Science and Technology, Av. Països Catalans 16, 43007 Tarragona, Spain. E-mail cbo@iciq.cat

[b] Dr. N. A. G. Bandeira
Centro de Química e Bioquímica, Faculdade de Ciências, Universidade de Lisboa, Campo Grande, 1749-016 Lisboa, Portugal

[c] Dr. N. A. G. Bandeira
Centro de Química Estrutural, Instituto Superior Técnico, Universidade de Lisboa, Avenida Rovisco Pais, 1049-001 Lisboa, Portugal

[d] Dr. V. Velasco, Dr. L. A. Barrios, Dr. D. Aguilà, Dr. G. Aromí
Departement de Inorgánica, Universitat de Barcelona, Diagonal 645, 08028, Barcelona, Spain. E-mail: guillem.aromi@qi.ub.es.

[e] Dr. S. J. Teat
Advanced Light Source, Berkeley Laboratory, 1 Cyclotron Road, Berkeley, California 94720, USA.

[f] Dr. O. Roubeau
Instituto de Ciencia de Materiales de Aragón (ICMA), CSIC and Universidad de Zaragoza, Plaza San Francisco s/n, 50009, Zaragoza, Spain.

[g] Dr C. Bo
Departament de Química Física i Inorgànica, Universitat Rovira i Virgili, Marcel·lí Domingo s/n, 43007 Tarragona, Spain

Abstract: The solid state and solution configuration of the heterodimetallic complexes, (Hpy)[LaEr(HL)$_3$(NO$_3$)(py)(H$_2$O)] (**1**), (Hpy)[CeEr(HL)$_3$(NO$_3$)(py)(H$_2$O)] (**2**), (Hpy)[CeGd(HL)$_3$(NO$_3$)(py)(H$_2$O)] (**3**) (Hpy)[PrSm(HL)$_3$(NO$_3$)(py)(H$_2$O)] (**4**) and (Hpy)$_2$[LaYb(HL)$_3$(NO$_3$)(H$_2$O)](NO$_3$) (**5**), where H$_3$L is 6-(3-oxo-3-(2-hydroxyphenyl)propionyl)pyridine-2-carboxylic acid, are analysed experimentally and through DFT calculations. Complexes **3**, **4** and **5** are described here for the first time, by means of single crystal X-ray diffraction and mass spectrometry. The theoretical study is also extended to the [LaCe] and [LaLu] analogues. The results are consistent with a remarkable selectivity of the metal distribution within the molecule while in the solid state, enhanced by the size difference of both ions. This selectivity is reduced in solution, especially for ions with the closest radii. This unique entry into 4*f*-4*f'* heterometallic chemistry for the first time establishes a difference between the selectivity in solution and that in the solid state, as a result of changes to the coordination numbers that follow the dissociation of terminal ligands upon dissolution of the complexes.

Introduction

The electronic structure of lanthanide elements is at the root of their very rich physico-chemical properties and their potential applications in a large variety of fields.[1] Some of the sophisticated uses of these elements rely on interactions with other metals within homo-[2] or heterometallic polynuclear molecular entities.[3] Of the latter category, the vast majority combine metal ions from different blocks of the periodic table (e.g., 3*d*-4*f*) within coordination clusters.[4] The reason is that these atoms are sufficiently different chemically, thus exhibiting disparate affinities for various ligand donor atoms or distinct preferred coordination geometries, which allows a selective distribution of different metals within segregated sites in a molecule. By contrast, the task of preparing heterometallic 4*f*-4*f'* molecular assemblies is much more challenging. Indeed, all the metals of the series are chemically very similar, since their valence electrons (4*f*) are shielded by the filled 5*s* and 5*p* electrons. A way to tackle this problem is through designed synthetic procedures carried out in several steps, where the different metals are sequentially incorporated,[5] or by linking preformed metal containing moieties.[6] Alternatively, one could during the course of one-pot reactions, exploit the size difference existing between any two different lanthanide ions as a result of the lanthanide contraction,[7] by using ligands with two types of coordination pockets, able to selectively discriminate different Ln(III) centers by their radius. This method has been employed with asymmetric ligands, L^1, conducing to the self-assembly of triple stranded dinuclear helicates of the type [Ln$_2$(L^1)$_3$] or [LnLn'(L^1)$_3$].[8] Similarly, a tritopic ligand L^2, capable of forming trinuclear helicates of the type [Ln$_3$(L^2)$_3$]$^{9+}$ was employed to obtain mixtures of heterometallic species [Ln$_x$Ln'$_{(3-x)}$(L^2)]$^{9+}$, with a central site exhibiting a higher affinity for larger metal ions than the distal positions.[9] A combination of H-NMR and spectrophotometry allowed to determine the formation constants of the various possible trinuclear species (x = 0,1,2,3) and assess the free energy favoring deviations from statistical distributions. These deviations are ascribed to differences in intramolecular electrostatic interactions and solvation effects (these latter, only relevant in solution).[10] On a different approach, the serendipitous self-assembly of Ln(III) ions with the bridging and chelating ligand quinolato, Q$^-$, produces clusters with formula [Ln$_3$Q$_9$] exhibiting two slightly different coordination sites, favoring larger ions at the central position of the molecule and smaller ions at the sides.[11] In all these cases, the purity of heterometallic analogues has not been reported to exceed 90%. The goal of preparing pure

heterometallic 4*f*-4*f*' molecular species remains a crucial challenge; it is bound to have a direct impact in relevant and diverse applications. Some of these are the optical up-conversion,[12] multimodal magnetic resonance imaging (MRI),[13] exploitation of sophisticated luminescence properties[14] or the realization of 2-qubit quantum gates for quantum computing.[15]

We previously reported an exhaustive, quasi-isostructural series of homometallic dinuclear lanthanide complexes with formulae $(Hpy)[Ln_2(HL)_3(NO_3)(py)(H_2O)]$ from the asymmetric ligand H_3L (H_3L = 6-(3-oxo-3-(2-hydroxyphenyl)propionyl)pyridine-2-carboxylic acid, Scheme 1).[16] Within these molecules, each metal exhibits a completely distinct coordination environment. A comprehensive structural analysis clearly shows the expected contraction with the Ln atomic number throughout the series. Most importantly, it also reveals that one position is systematically larger than the other for all the complexes. This is gauged by a consistent difference, *Δ*O, between average Ln–O distances at both sites. This feature clearly suggested the possibility of using this architecture for the synthesis of heterodimetallic [LnLn'] complexes. This was initially demonstrated with the preparation of the complex $(Hpy)[LaEr(HL)_3(NO_3)(py)(H_2O)]$ (**1**, [LaEr]), in addition to the [CeEr] (**2**), [CeY] and [LaY] counterparts.[17] We report here the new derivatives $(Hpy)[CeGd(HL)_3(NO_3)(py)(H_2O)]$ (**3**, [CeGd]), $(Hpy)[PrSm(HL)_3(NO_3)(py)(H_2O)]$ (**4**, [PrSm]) and $(Hpy)_2[LaYb(HL)_3(NO_3)(H_2O)](NO_3)$ (**5**, [LaYb]). Of all possible [LnLn'] combinations, the study was performed with a sample of compounds involving small, medium size and large Ln(III) ions, in addition of featuring large or small variations in ionic radius. The structural analysis of **1** to **5**, in comparison with the $[Ln_2]$ analogues (Ln = Ce, La, Pr, Sm, Gd, Er and Yb), confirms the selectivity for the heterometallic derivatives, which is superior in the solid state than in solution. This is corroborated with DFT calculations, performed on the structures observed in the solid state as well as the moieties detected through mass spectrometry (MS). From these results, it is inferred that in addition to differences in bond distances, the difference in coordination number at both sites (observed in the solid state and not in solution) constitutes another source of stabilization of the heterometallic fragment. This synergic effect had not been revealed previously and opens the door to synthetic strategies towards the production of purer and more diverse 4*f*-4*f*' assemblies.

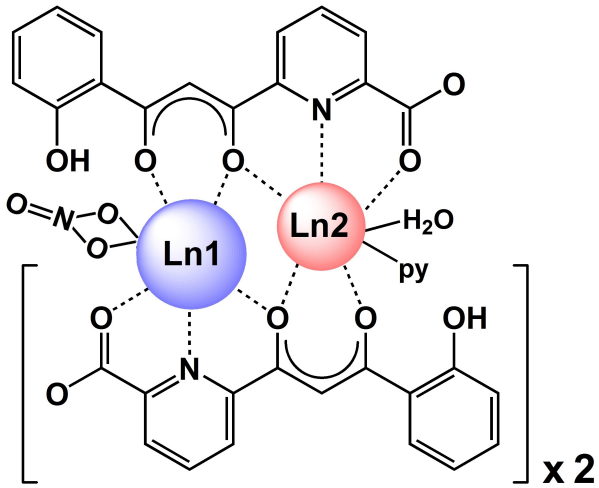

Scheme 1. Representation of the metal distribution around the dinuclear complexes of the $(Hpy)[Ln_2(HL)_3(NO_3)(py)(H_2O)]$ series, emphasizing two distinct coordination environments around Ln1 (larger site) and Ln2 (smaller site).

Results and Discussion

Synthesis

The new complexes $(Hpy)[CeGd(HL)_3(NO_3)(py)(H_2O)]$ (**3**), $(Hpy)[PrSm(HL)_3(NO_3)(py)(H_2O)]$ (**4**) and $(Hpy)_2[LaYb(HL)_3(NO_3)(H_2O)](NO_3)$ (**5**) were obtained as crystals in the same manner as the previously reported analogues. Thus, equimolar amounts of the corresponding $Ln(NO_3)_3$ salts were mixed in pyridine with the stoichiometric quantity of the ligand H_3L under aerobic conditions, and crystals were collected following the diffusion of Et_2O or toluene into the reaction mixture. The single-crystal X-ray diffraction structures are consistent with the proposed formulation (see below) and the elemental analyses, including these for the metals, are fully satisfactory. From these and previous reactions, it is observed that the yields vary from compound to compound (ranging from 10% for [PrSm] to the 70% of [CeY]), a reflection of the different tendencies for crystallization of each compound. The exact formulation of compound **5** reveals interesting differences with respect to the composition observed *hitherto* in this family of compounds as explained in detail below.

Description of Structures

(Hpy)[CeGd(HL)$_3$(NO$_3$)(py)(H$_2$O)] (3). Complex **3** crystallizes in the monoclinic space group $P2_1/c$ (Table 1). The unit cell contains four asymmetric units, each composed of one metal complex, one pyridinium cation hydrogen bonded to the latter and five lattice pyridine molecules. The complex moiety (Fig. 1) exhibits the structure observed consistently for this family of compounds;[16a, 17] it is anionic and it is composed of two Ln(III) metal ions (one of Ce and one of Gd) bridged by and chelated by three HL^{2-} ligands, the latter showing two opposite orientations with respect to the Ce···Gd vector. This causes two different coordination environments around each metal; Ce(III) is chelated by two (O,N,O) pockets and one (O,O) moiety, whereas Gd(III) is bound to two bidentate and one triatomic coordination unit (Scheme 1). The coordination number (CN) of ten around Ce is completed by a bidentate NO_3^- ligand, whereas CN of nine around Gd is reached with the concurrent coordination of one pyridine and one water ligand.

Table 1. Crystallographic and refinement parameters for the structures of compounds **3**, **4** and **5**.

Compound	**3**	**4**	**5**
Formula	$C_{80}H_{65}CeGdN_{11}O_{19}$	$C_{75}H_{62}N_{10}O_{20}PrSm$	$C_{80}H_{68}LaN_{12}O_{23}Yb$
FW (g mol^{-1})	1781.80	1714.62	1877.42
Wavelength (Å)	0.77490	0.77490	0.71073
T (K)	100	150	101
Crystal system	monoclinic	monoclinic	triclinic
Space group	$P2_1/c$ (nº 14)	$P2_1/c$ (nº 14)	$P\bar{1}$ (nº 2)
a (Å)	14.4859(13)	14.944(2)	14.5730(8)
b (Å)	15.7852(14)	15.664(2)	15.8941(10)
c (Å)	35.855(3)	32.606(4)	16.5429(10)
α (°)	90	90	91.850(3)
β (°)	113.393(3)	110.857(5)	99.754(3)
γ (°)	90	90	92.299(3)
V (Å^3)	7524.8(11)	7132.4(16)	3770.3(4)
Z	4	4	2
ρ_{calcd} (g cm^{-3})	1.573	1.597	1.654
μ (mm^{-1})	1.938	1.964	1.880
Independent reflections (R_{int})	22918 (0.0395)	10885 (0.0390)	15079 (0.0508)
Restraints / Parameters	194 / 1006	267 / 1006	26 / 1061
Goodness-of-fit on F^2	1.040	1.162	1.118
Final R_1 / wR_2 [$I>2\sigma(I)$]	0.0396 / 0.1015	0.0341 / 0.0835	0.0338 / 0.0793
Final R_1 / wR_2 [all data]	0.0504 / 0.1069	0.0406 / 0.0877	0.0479 / 0.0924
Largest diff. peak and hole (e Å^3)	1.572 / –1.341	1.616 / –1.202	1.368 / –1.665

The average of the Ln−O distances (Table 2), <Ln–O>, (O from HL^{2-} ligands) are 2.524 Å (Ce) and 2.406 A (Gd), thus leading to ΔO = 0.12 Å (Fig. 2). In the previously reported homodimetallic [Ce_2] analogue, the <Ce−O> values are 2.524 and 2.481 Å (ΔO = 0.043 Å), respectively, whereas the corresponding parameters for the [Gd_2] derivative are 2.430 and 2.404 A (ΔO = 0.026 Å).[16a] The intermetallic Ce···Gd distance is 3.878 Å, compared with 3.9286(5) and 3.8038(11), respectively, for the [Ce_2] and [Gd_2] compounds. These figures clearly show that in compound **3**, Ce and Gd have selectively taken their preferred position based on their size difference (ionic radii, r_{Ln},[18] in Å of r_{Ce} = 1.220 and r_{Gd} = 1.105, Δr = 0.115). This is supported by the fact that any other distribution of Ce and/or Gd leads to data refinements with unreasonable displacement parameters and bad agreement factors. This assignment is consistent with the results from DFT calculations (see below).

The phenol hydrogen atoms of HL^{2-} were localized crystallographically. The short N3S-O2 distance is evidence of the presence of a hydrogen bond between these atoms, since it is smaller than the sum of their van der Waals radii (Table 3). The existence of a pyridinium cation (Hpy^+; N3S in Fig. 1) coordinated to the $-COO^-$ group of one of the HL^{2-} ligands was also demonstrated by DFT as discussed below. Complex **3** is chiral and both enantiomers are present within the unit cell, which is then racemic.

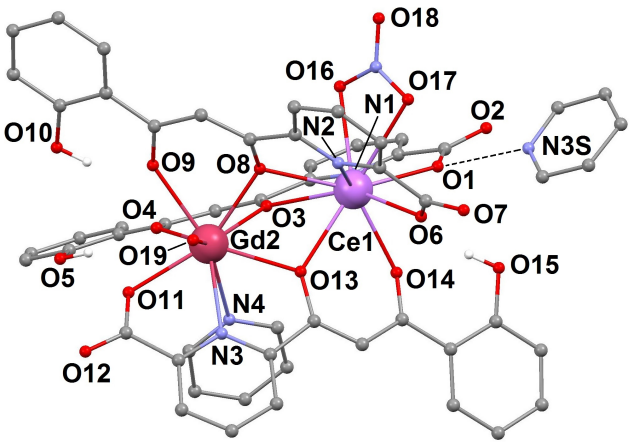

Figure 1. Molecular structure of (Hpy)[CeGd(HL)$_3$(NO$_3$)(py)(H$_2$O)] (**3**), emphasizing the hydrogen bond established between one of its –COO$^-$ groups and a pyridinium cation. All heteroatoms are labelled, C atoms are in grey and only H atoms of the phenol groups shown in white.

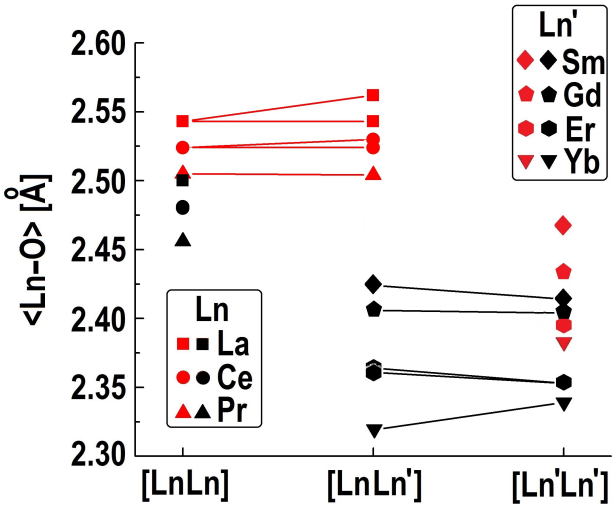

Figure 2. Plot of <Ln−O> values for various (Hpy)[Ln$_2$(HL)$_3$(NO$_3$)(py)(H$_2$O)] complexes (Ln = La, Ce, Pr, Sm, Gd, Er, Yb),[16a] together with the values for **1** ([LaEr]), **2** ([CeEr]), **3** ([CeGd]), **4** ([PrSm]) and **5** ([LaYb]). Red and black symbols are values por the large and small positions, respectively (Ln1 and Ln2, respectively, in Scheme 1). Lines link parameters for metal ions occupying the same position in both, the heterometallic complexes and the corresponding homometallic analogue.

(Hpy)[PrSm(HL)$_3$(NO$_3$)(py)(H$_2$O)] (4). Compound **4** crystallizes in the same space group as **3** ($P2_1/c$, Table 1). The unit cell and asymmetric unit are analogous, now with one lattice molecule of water instead of one of the crystallization molecules of pyridine. The structure of the [PrSm] complex cation (Fig. 3) is the same as the cation of **3**, only with small structural changes derived from the different identity of the metals. Here, <Pr–O> and <Sm–O> are 2.504 Å and 2.424 A, respectively (ΔO = 0.08 Å, Fig. 2). These values are to be compared with the analogous parameters for the corresponding homodimetallic species, which are 2.505 and 2.456 Å (ΔO = 0.049 Å) for [Pr$_2$], and 2.468 and 2.414 A (ΔO = 0.054 Å) for [Sm$_2$]. The intermetallic distances within [PrSm], [Pr$_2$] and [Sm$_2$] are 3.8567(5), 3.8941(6) and 3.8197(13) Å, respectively. The above comparisons show that Pr(III) takes the position corresponding to Ln1 (Scheme 1) and Sm resides at the location of Ln2, as determined by their respective sizes (r_{Pr} = 1.200 and r_{Sm} = 1.140 Å; Δr = 0.06).[18] Again, the refinement of the crystallographic data and DFT calculations (see below) using other metal distributions confirm the selective nature of this heterometallic species.

Table 2. Selected bond lengths (Å) and angles (º) describing the coordination environments of the Ln sites as well as the Ln···Ln' separation in the structures of compounds **2** and **3**, obtained both, experimentally and through DFT calculations.

2			**3**		
		DFT			DFT
Sm1–O4	2.369(3)	2.419	Yb1–O8	2.258(2)	2.310
Sm1–O11	2.393(3)	2.376	Yb1–O4	2.273(2)	2.312
Sm1–O8	2.429(3)	2.459	Yb1–O9	2.293(3)	2.355
Sm1–O3	2.434(3)	2.455	Yb1–O19	2.297(2)	2.508
Sm1–O13	2.451(3)	2.558	Yb1–O11	2.343(2)	2.369
Sm1–O9	2.467(3)	2.572	Yb1–O3	2.367(2)	2.364
Sm1–O19	2.476(3)	2.709	Yb1–O13	2.381(3)	2.410
Sm1–N3	2.524(4)	2.566	Yb1–N3	2.397(3)	2.450
Sm1–N5	2.735(4)	2.726			
Pr2–O1	2.435(3)	2.315	La2–O14	2.439(3)	2.467
Pr2–O6	2.445(3)	2.333	La2–O1	2.471(2)	2.408
Pr2–O14	2.481(3)	2.538	La2–O6	2.488(2)	2.536
Pr2–O13	2.485(3)	2.529	La2–O8	2.585(3)	2.666
Pr2–O8	2.509(3)	2.653	La2–O17	2.648(3)	2.609

Pr2–O18	2.590(3)	2.545	La2–O13	2.673(2)	2.765
Pr2–N2	2.632(4)	2.686	La2–N2	2.676(3)	2.734
Pr2–O3	2.667(3)	2.770	La2–O3	2.715(2)	2.815
Pr2–N1	2.703(4)	2.723	La2–N1	2.717(3)	2.741
Pr2–O16	2.705(4)	2.509	La2–O16	2.722(3)	2.644
Sm1···Pr2	3.8567(5)	4.035	Yb1···La2	3.8784(3)	3.977
Sm1–O3–Pr2	98.13(10)	100.9	Yb1–O3–La2	99.24(7)	100.0
Sm1–O8–Pr2	102.71(11)	104.2	Yb1–O8–La2	106.21(9)	105.9
Sm1–O13–Pr2	102.75(10)	105.0	Yb1–O13–La2	100.07(9)	100.2

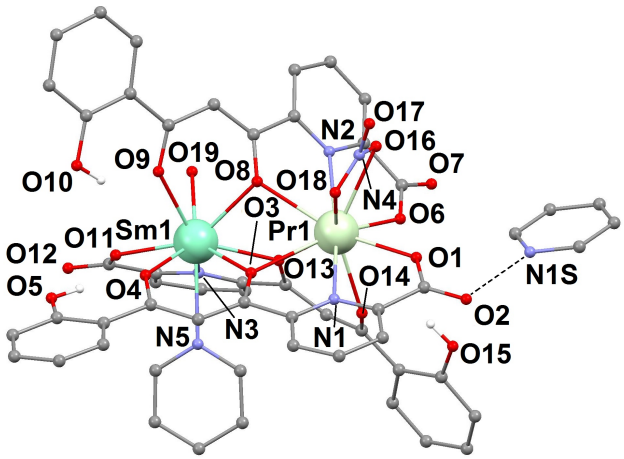

Figure 3. Molecular structure of [PrSm(HL)$_2$(H$_2$L)(NO$_3$)(py)(H$_2$O)] (**4**), emphasizing the hydrogen bond established between its –COOH group and a lattice pyridine molecule. All heteroatoms are labelled, C atoms are in grey and only H atoms of the phenol groups shown in white.

$(Hpy)_2[LaYb(HL)_3(NO_3)(H_2O)](NO_3)$ (5). Compound **5** crystallizes in the triclinic space group *P*-1 (Table 1). The asymmetric unit contains the atoms of the title empirical formula, in addition to five lattice pyridine molecules and one of water. The unit cell contains two asymmetric units. The complex anion in **5** (Fig. 4) is formed by two metal ions (La and Yb) wrapped by three deprotonated H_3L ligands (as HL^{2-}) in two opposite orientations with respect to the metal axis. Therefore, the complex is negatively charged (–1) as all the other related complexes studied *hitherto*. Similarly, the disposition of the ligands creates two coordination sites. Here, the large position contains the metal ion La(III), coordinated through one (O,O) chelating unit and two (O,N,O) ones, in addition to the NO_3^- ligand, which is bidentate (CN=10). The Yb(III) ion features two (O,O) pockets and one (O,N,O) chelating group, in addition to only one molecule of H_2O. Therefore, it is the first time that one complex of this family does not show a pyridine ligand, yielding a CN of eight for Yb(III). Another major difference here is the presence of two Hpy^+ cations instead of one, hydrogen bonded to the anion of **5**. The additional positive charge is compensated by a NO_3^- counter ion. In this complex, <La−O> = 2.562 Å and <Yb−O> = 2.319 Å (ΔO = 0.243 Å). The more pronounced difference between both sites (Fig. 3) is a consequence of a larger disparity of metal ionic radii (r_{La} = 1.250 and r_{Yb} = 1.010, Δr = 0.24). It is pertinent to compare the Ln–O parameters with these from the [La_2] and [Yb_2] analogues, keeping in mind that in the latter, the CN of the metal at site 2 is nine, and not eight, because of the terminal pyridine ligand (not present in **5**). These parameters are, in Å, <La1−O> = 2.543 and <La1−O> = 2.500 (Δr = 0.043) for [La_2] and <Yb1−O> = 2.378 and <Yb2−O> = 2.339 (Δr = 0.039) for [Yb_2]. The comparison indicates again the selectivity of the [LaYb] system of **5**. This is seen also in comparing the intermetallic distances of 3.878 Å in **5** when compared with 3.9590(13) and 3.741(4) Å of [La_2] and [Yb_2], respectively. The structural refinement fully supports the metal assignment, which is consistent with the DFT results (see below).

Table 3. Distances and angles describing the hydrogen bonds in the structures of compounds **3**, **4** and **5**.

D–H···A	D–H (Å)	H···A (Å)	D···A (Å)	D–H···A (º)
3				
O5–H5···O4	0.84	1.83	2.557(4)	144.3
O10–H10···O9	0.84	1.81	2.536(4)	144.3
O15–H15···O14	0.84	1.90	2.617(5)	142.6
O19–H19D···N1S	0.876(19)	1.89(2)	2.760(5)	170(4)
O19–H19C···N2S	0.893(19)	1.91(2)	2.799(4)	175(4)
4				
O5–H5···O4	0.84	1.88	2.590(5)	141.7
O10–H10···O9	0.84	1.79	2.526(4)	144.8
O15–H15···O14	0.84	1.90	2.600(4)	140.0
O19–H19B···N5S	0.86(7)	1.95(7)	2.808(6)	177(6)
O19–H19C···N6S#1	0.84(7)	1.99(7)	2.810(6)	165(6)
O1W–H1W···O12	0.92(2)	1.97(2)	2.891(7)	189(12)
O1W–H2W···O7#2	0.93(2)	2.21(3)	3.029(7)	146(5)
N1S–H1SB···O2	0.88	1.81	2.684(6)	176.3
N2S–H2SB···O1	0.88	1.82	2.686(6)	168.0
5				
O5–H5···O4	0.84	1.85	2.575(3)	144.2
O10–H10···O9	0.84	1.83	2.549(4)	142.9
O15–H15···O14	0.84	2.03	2.718(4)	139.1
O19–H19A···N2S	1.04	1.83	2.725(4)	141.3
O19–H19B···N6S#3	1.03	1.75	2.763(4)	164.7
O1W–H1WA···O2N#4	0.87	2.11	2.869(8)	145.9
O1W–H1WB···O1N	0.87	2.40	2.778(8)	106.9
N1S–H1S···O12	0.88	1.74	2.615(5)	176.5
N3S–H3SA···O2	0.88	1.75	2.630(4)	177.2

Symmetry operations: #1: 1-x, 0.5+y, 0.5-z; #2:1-x, y-0.5, 0.5-z; 1-x, 1-y, 1-z; #-x, 2-y, 1-z

In analogy with **1** to **4**, the two pyridinium cations (Hpy^+; N3s and N1S in Fig. 2) in **5** are inferred by their proximity to two $–COO^-$ groups from two HL^{2-} ligands and the presence electron density near N3s and N1S. The [LaYb] complex cation is chiral, both enantiomers being present within the unit cell as a racemic mixture.

The relative <Ln−O> values plotted in Fig. 2 reproduce perfectly the structural expectations for the [LnLn'] systems, in light of their comparison with the corresponding [Ln_2] or [Ln'_2] counterparts. In this respect, relevant observations are; *i*) for all compounds, the values of <Ln−O> are consistent with the lanthanide contraction, when comparing Ln ions on equivalent positions (*ie*., in terms of size, La>Ce>Pr>Sm>Gd>Er>Yb), *ii*) for all compounds, a ΔO gap is maintained between the large coordination site and the small one, *iii*) ΔO is wider as Δr becomes larger, *iv*) in heterometallic compounds, <Ln−O> for a given position is closest to the corresponding value of the predicted metal when occupying this position in the homometallic analogue (red and black colors for the large and small positions, respectively; Ln1 and Ln2 in Scheme1). This excellent agreement with the expected behavior, also in line with the predictions from the lanthanide contraction, supports the high selectivity of this architecture for specific heterometallic dispositions.

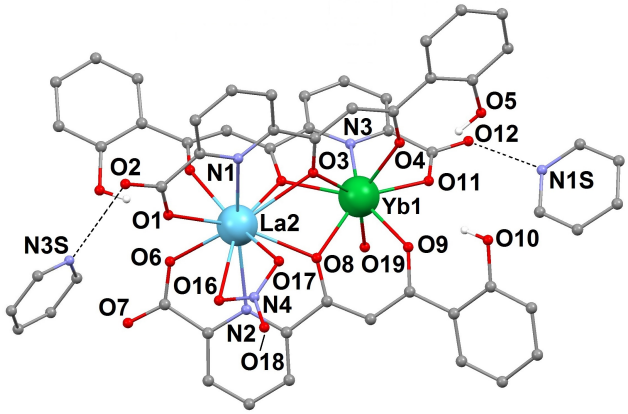

Figure 4. Molecular structure of the complex cation of $(Hpy)_2[LaYb(HL)_3(NO_3)(H_2O)](NO_3)$ (**5**), emphasizing the hydrogen bonds established between two of its $-COO^-$ groups and two pyridinium cations. All heteroatoms are labelled, C atoms are in grey and only H atoms of the phenol groups shown in white.

Mass Spectrometry

Electrospray ionization mass spectrometry (ESI-MS) was used as a powerful technique to assess the integrity of the solid state structure in solution, and ascertain whether the metal distribution observed by X-ray diffraction was maintained. Thus, for complex $(Hpy)[CeGd(HL)_3(NO_3)(py)(H_2O)]$ (**3**), the spectrogram shows a prominent peak with *m/z* of 1147.98, fitting the isotopic distribution within the fragment $[CeGd(HL)_2(H_2L)]^+$ (Fig. 4), in line with the formulation extracted from the crystal. However, peaks for homometallic fragments $[Ce_2(HL)_2(H_2L)]^+$ (1129.96) and $[Gd_2(HL)_2(H_2L)]^+$ (1166.00) are also detected. Complex $(Hpy)[PrSm(HL)_3(NO_3)(py)(H_2O)]$ (**4**) exhibits a similar behavior, featuring dinuclear species mainly corresponding to $[PrSm(HL)_2(H_2L)]^+$ (1142.98), $[Sm_2(HL)_2(H_2L)]^+$ (1151.01) and $[Pr_2(HL)_2(H_2L)]^+$ (1131.97). Here the relative presence of homometallic fragments is even more prominent than with **3**. This shows that these compounds in solution, especially the latter, undergo a process of scrambling and exhibit metal distributions different from these seen in the solid state. Therefore, in the absence of the terminal ligands (NO_3^-, H_2O and py), ligands H_2L^- and HL^{2-} lose selectivity in distributing ions according to their size. The selectivity in solution, however, increases with the magnitude of Δr (thus, it is larger for [CeGd], with $\Delta r = 0.115$ Å, than for [PrSm], $\Delta r = 0.06$ Å). Interestingly, the high selectivity of the structure observed in the solid state, together with the diminished selectivity of the system when the terminal ligands are removed is also predicted by DFT calculations (see below). In contrast with **3** and **4**, the ESI-MS spectrogram of complex $(Hpy)_2[LaYb(HL)_3(NO_3)(H_2O)](NO_3)$ (**5**) shows a dominating signal with *m/z* of 1162.99, with the right isotopic multiplicity for the fragment $[LaYb(HL)_2(H_2L)]^+$, this time in the almost complete absence of any of the homometallic counterparts. These observations are consistent with the fact that the metals of **3** exhibit much larger size disparity ($\Delta r = 0.24$ Å) and thus, high selectivity for a specific heterometallic distribution, even in solution and for the species without terminal ligands. This is also predicted by DFT calculations, in addition to a much higher drive for the [LaYb] metal arrangement in the structure observed in the solid state. The same experiments previously performed on the [LaEr] and [CeEr] analogues also revealed the exclusive preference for the heterometallic association, both in the solid state and in solution, for $(Hpy)[LaEr(HL)_3(NO_3)(py)(H_2O)]$ (**1**) and $(Hpy)[CeEr(HL)_3(NO_3)(py)(H_2O)]$ (**2**).[17]

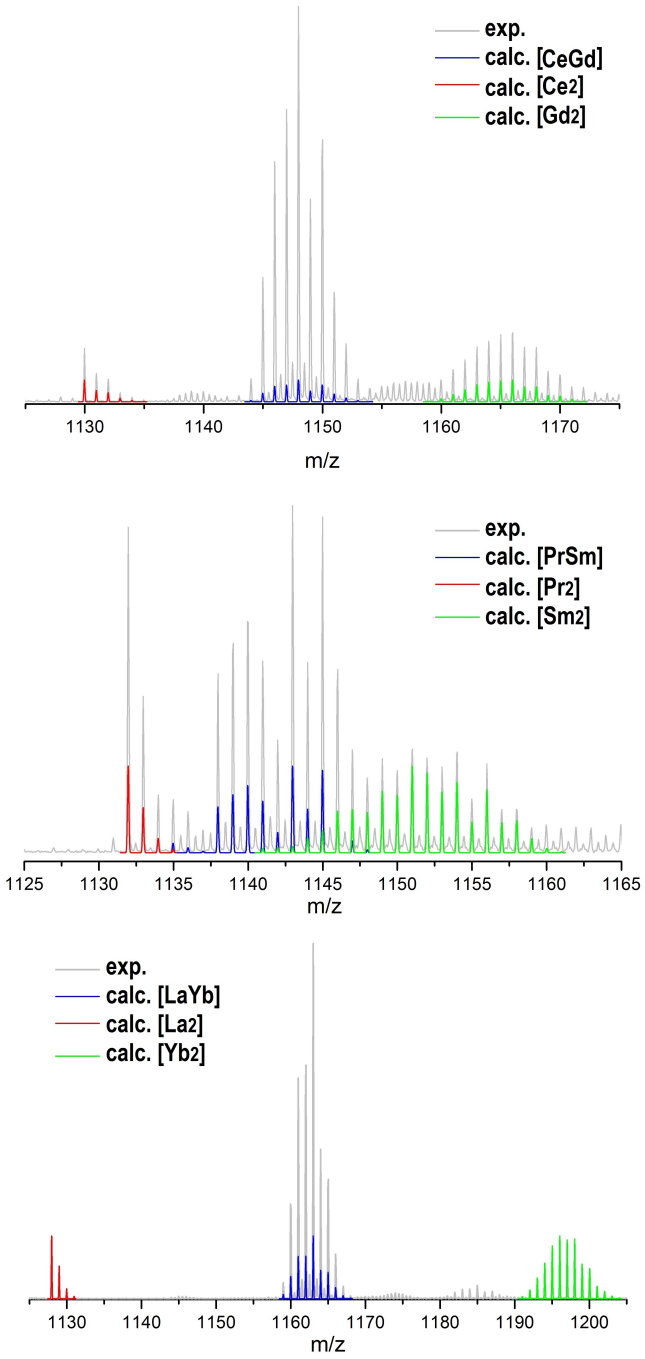

Figure 5. Selected regions of the experimental (grey line) ESI-MS spectrograms of **2** (top) and **3** (bottom) and simulated signals of various $[LnLn'(HL)_2(H_2L)]^+$ fragments (colored lines, see legend for metals) showing the corresponding isotopic distributions.

DFT Studies

DFT based methods were used to rationalize the selectivity in the metal distribution of the [LnLn'] complexes. First, the energy of two structures analogous to those seen in Scheme 1 were compared for various Ln1/Ln2 pairs. One structure bears Ln1 and Ln2 as experimentally observed (structure A, Fig. 6), and the other had the identity of the Ln ions inverted (structure B, Fig. 6). The three ligands were computed in the HL^{2-} form, as seen in the solid state, thus, the complexes always bearing an overall negative charge of –1 and formula $[LnLn'(HL)_3(NO_3)(py)(H_2O)]^-$, with the NO_3^- ligand always bound in a chelating fashion. This structure is consistent with the O-C bond lengths of the carboxylate groups of the HL^{2-} ligands determined by X-ray diffraction, which showed them to be

quasi identical. In order to ascertain the position of the putative protons involved in hydrogen bonding, both possible arrangements, RCOOH···py and $RCOO^{-}\cdots Hpy^{+}$ were analyzed. Indeed, an energy minimum was only identified for the latter. The metal pairs investigated were the five experimentally studied combinations [CeEr], [PrSm], [LaYb], [LaEr] and [CeGd] in addition to the hypothetical [LaCe] and [LaLu] systems. The latter two correspond to two similar ions with large and similar radii and two ions with contrasting radii respectively. The ligand-metal bond lengths of the DFT optimized structures are slightly longer compared with these of the crystallographic structures (Table 2) but no other significant geometric changes are otherwise observed from the bond distances. Alternatively, using the SHAPE program we have determined the polyhedral coordination of each metal site for [CeEr], [PrSm] and [LaYb] through Continuous Shape Measures (CShM's). [19] The obtained results are collected in Table S1 in the *Supporting Information*. With this method different polyhedral sizes are observed in all the complexes as a function of CN where each ligating atom corresponds to a vertex.Hence Pr, Ce and La have a CN=10 (10 vertex), Sm and Er have nine, and Yb eight. A match between the X-Ray and the DFT coordination polyhedra was found for structures with CN eight and nine, wherefore Yb is a *Biaugmented trigonalprism*, Er a *Spherical tricapped trigonal prism* and Sm is a *Capped square antiprism.* Regarding CN=10 slight differences are observed between the X-Ray and DFT polyhedra (Table S1 and Figure S3). In all cases, the complexes were considered with their maximum possible spin multiplicity. The geometry optimization was performed for all the structures. The energy differences between structures A and B for all the compounds (ΔE_{AB}) are collected on Table 4. It can be seen that with no exception, structure A is favored over B. Thus, the calculations predict that the larger metal has a preference for the site engaging one (O,O) and two (O,N,O) pockets, featuring CN = 10, while the smaller metal accommodates at the position with two (O,O) and one (O,N,O) moieties, with CN = 9. Indeed, ΔE_{AB} is correlated with the difference in ionic radii of both metals, Δr, which is at the root of this selectivity. Since the structure of **3** ([LaYb]) does not incorporate the ligand pyridine, the Yb(III) ion thus exhibiting CN = 8, ΔE_{AB} was also calculated for its real geometry. The stabilization of structure A with no pyridine was found to be 36% higher. This is consistent with the experimental findings, which show that **3** does not incorporate pyridine, despite being the solvent of the reaction. In order to understand the experimental results from the solution studies, optimized structures C and D related to the species detected by ESI-MS were also computed; specifically, the moieties $[LnLn'(HL)_3]$ (Fig. 6, bottom), which incorporate no terminal ligands. The results show that now the relative stability, ΔE^*_{CD}, is much smaller in all cases, resulting in a significantly less pronounced selectivity. All the ΔE^*_{CD} values are marginally positive except for [PrSm] for which the favoured arrangement is even reversed, also by a likewise small amount (-1.1 $kcal.mol^{-1}$). The quasi cancelation of the selectivity for this derivative in this configuration is fully consistent with the experimental observations in solution. This corroborates that the effect of metal size in directing the selective disposition of the lanthanide ions within the [LnLn'] species is much more marked for the structure observed in the solid state than that detected in solution, as observed experimentally.

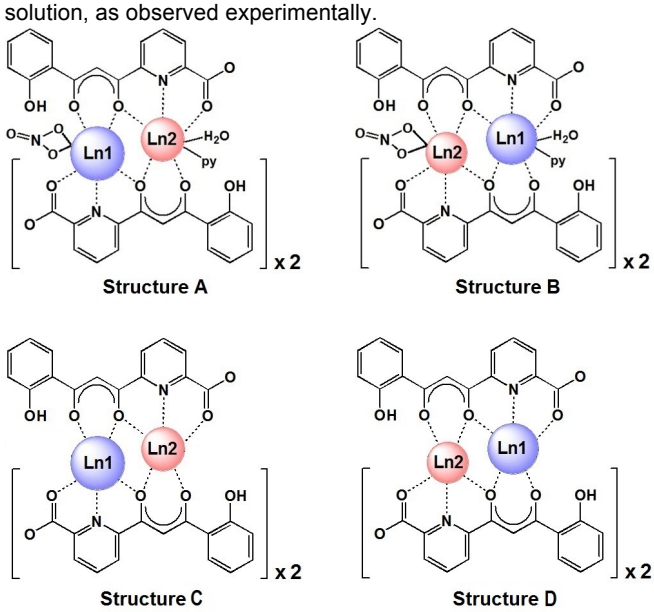

Figure 6. Schematic representation of the fragments $[LnLn'(HL)_3(NO_3)(py)(H_2O)]^{-}$ used in the DFT calculations, emphasizing the experimental structure, with the larger (Ln1) and smaller (Ln2) metal occupying the bigger and smaller coordination site, respectively (Structure A) and the arrangement with both metals exchanged (Structure B), and of the fragments $[LnLn'(HL)_3]^{-}$ (thus, without terminal ligands) also computed, with both distributions of metals (Structures C and D).

Table 4. Calculated energy differences gauging the selectivity of the [LnLn'] species in relation to compared ionic radii.

[LnLn']	ΔE_{AB}[a]	ΔE^*_{CD}[c]	ΔH_{form}[d]	Δr[e]
[LaLu]	11.6		-16.91	0.255
[LaYb]	8.6 (11.7)[b]	1.2	-11.63	0.240
[LaEr]	8.9		-28.37	0.210
[CeEr]	7.5	3.6	-14.14	0.180
[CeGd]	6.3		-11.44	0.115
[PrSm]	2.6	-1.1	-11.95	0.060
[LaCe]	1.0		-3.37	0.030

[a] If not said otherwise, energy difference between structures A and B in Fig. S1 (kcal·mol^{-1}). [b] Energy difference using the structure seen for this compound by X-ray diffraction, *ie.* without one pyridine ligand. [c] Energy difference using structures without terminal ligands as in Fig. S2. [d] Energy of the reaction in Eq. 1 (kcal·mol^{-1}). [e] Ionic radii difference of the metals involved[18] (Å).

The energy of formation of all compounds from the corresponding homodimetallic analogues, ΔH_{form}, (Eq. 1) was also calculated.

$$[Ln_2(HL)_3(py)(H_2O)](NO_3) + [Ln'_2(HL)_3(py)(H_2O)](NO_3) \downarrow \quad (1)$$

$$2[LnLn'(HL)_3(py)(H_2O)](NO_3)$$

In all cases, the formation of the heterometallic species is favored (Table 4, column 4), with energies that exceed approximately by a factor of five these determined for hetero-lanthanide coordination helicates.[9] Here, the correlation with Δr is not so clear, therefore, other aspects, relative to the stability of the corresponding homometallic assemblies must also play a role. In any case, the results from all the calculations support the experimental data, since they reflect a clear selectivity and preference for the formation of the heterodimetallic species in the solid state, which is much less pronounced in solution.

Conclusions

In the presence of lanthanide nitrates, the multidentate ligand H_3L systematically leads to the formation of dinuclear complexes with formula $(Hpy)[Ln_2(HL)_3(NO_3)(py)(H_2O)]$, featuring two distinct metal coordination sites. If combinations of two different $Ln(NO_3)_3$ salts are used, the system yields pure heterodimetallic molecules with the analogous structure, distributing both metal ions, selectively among both distinct coordination sites, according to their size. The selectivity is diminished in solution when this size difference is reduced, as detected by MS spectrometry, which shows that metals with very similar cationic radii feature other metal distributions within the molecular scaffold. This can be corroborated through DFT calculations, which confirms that a combination of different <Ln–O> values and terminal ligands, as observed in the solid state, ensures a very high selectivity that cannot be maintained in solution, as a result of the dissociation or lability of the terminal ligands. These findings confirm the great potential of a simple synthetic tool for the production of [LnLn'] molecules with any combination of two lanthanide ions and also the suitability of DFT based methods for rationalizing the observed selectivity of the ligand coordination sites in the [LnLn'] complexes, both in the solid state and in solution.

Experimental Section

Synthesis

$(Hpy)[CeGd(HL)_3(NO_3)(py)(H_2O)]$ (3). A yellow solution of H_3L (30 mg, 0,105 mmol) in pyridine (10 ml) was added dropwise into a colourless solution of $Ce(NO_3)_3{\cdot}6H_2O$ (15.2 mg, 0.035 mmol) and $Gd(NO_3)_3{\cdot}6H_2O$ (15.8 mg, 0.035 mmol) in pyridine (10 ml). The mixture was stirred for one hour, and the resulting orange solution was layered with toluene. After two weeks, yellow crystals of **3** were obtained in 53 % yield. Anal Calcd (Found) for **3**·1.5y4.2H_2O (considering a 1:1 Ce:Gd ratio): C 43.08 (42.74), H 3.48 (2.59), N 5.26 (5.69). MS: *m/z* = 1147.98, $[CeGd(HL)_2(H_2L)]^+$; 1129.96; $[Ce_2(HL)_2(H_2L)]^+$, 1166.00; $[Gd_2(HL)_2(H_2L)]^+$. IR (KBr pellet, cm-1): 3407 mb, 1618 s, 1584 s, 1557 m, 1528 s, 1463 m, 1396 s, 1384 s, 1299 m, 1242 w, 1202 w, 1121 w, 1058 w, 949 w, 891 w, 758 w, 706 w, 665 w, 635 w, 569 w.

(Hpy)[PrSm(HL)$_3$(NO$_3$)(py)(H$_2$O)] (4). A yellow solution of H_3L (30 mg, 0,105 mmol) in pyridine (10 ml) was added dropwise into a colourless solution of $Pr(NO_3)_3{\cdot}6H_2O$ (15.2 mg, 0.035 mmol) and $Sm(NO_3)_3{\cdot}6H_2O$ (15.6 mg, 0.035 mmol) in pyridine (10 ml). The mixture was stirred for one hour, and the resulting orange solution was layered with Et_2O. After one week, yellow crystals of **4** were obtained in 10 % yield. Anal Calcd (Found) for **4**·4.2H_2O(-0.9py) (considering a 1:1 Sm:Pr ratio): C 43.66 (43.47), H 3.23 (3.02), N 5.14 (5.38). Metal analysis (moles Pr/ moles Sm); 0.98. ESI MS: *m/z* = 1144.98 $[PrSm(HL)_2(H_2L)]^+$; 1151.01, $[Sm_2(HL)_2(H_2L)]^+$; 1131.97, $[Pr_2(HL)_2(H_2L)]^+$. IR (KBr pellet, cm-1): 3384 mb, 1618 s, 1584 s, 1559 m, 1529 s, 1464 m, 1401 s, 1384 s, 1324 m, 1300 m, 1240 w, 1202 w, 1148 w, 1121 w, 1059 w, 951 w, 891 w, 754 w, 707 w, 664 w, 636 w, 569 w.

(Hpy)$_2$[LaYb(HL)$_3$(NO$_3$)(H$_2$O)](NO$_3$) (5). A yellow solution of H_3L (30 mg, 0.105 mmol) in pyridine (10 ml) was added dropwise onto a colourless solution of $Yb(NO_3)_3{\cdot}5H_2O$ (15.8 mg, 0.035 mmol) and $La(NO_3)_3{\cdot}6H_2O$ (15.2 mg, 0.035 mmol) in pyridine (10 ml). The mixture was stirred for one hour, and the resulting yellow/orange solution was layered with Et_2O. After one week, orange crystals of **5** were obtained in 38% yield. Anal Calcd (Found) for **5**·3.1H_2O(-1.9)py: C 41.86 (41.98), H 2.76 (2.91), N 4.4 (4.24). Metal analysis (moles La/ moles Yb); 1.00. ESI MS: *m/z* = 1162.99 $[LaYb(HL)_2(H_2L)]^+$. IR (KBr pellet, cm-1): 3384 mb, 1616 s, 1583 s, 1557 m, 1526 s, 1462 m, 1401 s, 1385 s, 1323 m, 1299 m, 1240 w, 1202 w, 1147 w, 1120 w, 1057 w, 949 w, 890 w, 757 w, 706 w, 664 w, 634 w, 568w.

X-Ray Crystallography

Data for compound **4** were collected at 150 K with a Bruker APEX II CCD diffractometer on the Advanced Light Source beamline 11.3.1 at Lawrence Berkeley National Laboratory, from a silicon 111 monochromator (λ = 0.7749 Å) on a yellow needle with dimensions 0.18 x 0.02 x 0.02 mm^3. Data for compound **5** were collected at 101 K on a Bruker APEXII QUAZAR diffractometer equipped with a microfocus multilayer monochromator with MoKα radiation (λ = 0.71073 Å) on a yellow needle with dimensions 0.32 x 0.03 x 0.02 mm^3. Data reduction and absorption corrections were performed with SAINT and SADABS, respectively.[20] Both structures were solved by SHELXS[21] and refined by full-matrix least-squares on F^2 with SHELXL-2014.[22] The heterometallic nature of the asymmetric unit in compound **5** is clearly indicated by the worse agreement factors unrealistic relative displacement parameters of an homometallic composition, either La_2 or Yb_2. For compound **4**, the heterometallic composition cannot be confirmed unambiguously on sole basis of the structural data, since replacing Sm by Pr and Pr by Sm does not result in significant modifications of the agreement factors, even though the best situation remains that of the present heterometallic structural model. In both compounds, the relative position of each lanthanide ion is confirmed by the much poorer final agreement factors and worse or even unreasonable relative displacement parameters resulting from inverted relative positions. The Ln−O bond distances, compared to these on the homometallic counterparts confirm also the assignement. All details can be found in CCDC 1520532 (**5**) and CCDC 1520533 (**4**) that contain the supplementary crystallographic data for this paper. These data can be obtained free of charge from The Cambridge Crystallographic Data Center via https://summary.ccdc.cam.ac.uk/structure-summary-form. Crystallographic and refinement parameters are summarized in Table S1. Selected bond lengths and angles and intermolecular distances are given in Tables S2 and S3.

Experimental Details. IR spectra were recorded on KBr pellets, in the range 4000-400 cm^{-1}, with a Thermo Nicolet Avatar 330 FT-IR spectrometer. Elemental analyses were performed with a Perkin-Elmer Series II CHNS/O Analyser 2400 at the Servei de Microanàlisi of the CSIC, Barcelona. Positive ion ESI mass spectrometry experiments were performed on a LC/MSD-TOF (Agilent Technologies) with a dual source equipped with a lock spray for internal reference introduction, at the Unitat d'Espectrometria de Masses (SSR) of the University of Barcelona. The experimental parameters were: capillary voltage 4 kV, gas temperature 325ºC, nebulizing gas pressure 15 psi, drying gas flow 7.0 L min^{-1}, and fragmentor voltage ranging from 175 to 250 V. internal reference masses were *m*/*z* 121.05087 (purine) or 922.00979 (HP-0921). Samples (microlitres) were introduced into the source by a HPLC system (Agilent 1100), using a mixture of H_2O/CH_3CN (1/1) as eluent (200 µL min^{-1}).

Computational Details. Geometries for the calculations were fully optimized using a DFT method by employing the ADF program (Scientific Computing and Modelling ADF-2013.01, http://www.scm.com) The Becke [23] and Perdew [24] gradient-corrected exchange and correlation functionals (BP86), respectively, were used in the calculations. The ZORA [25] scalar relativistic Hamiltonian was employed with a TZP basis set[25a] for the metal atoms, oxygen and nitrogen, and DZP basis set for carbon and hydrogen atoms). The geometry optimizations were performed with the default numerical integration scheme of Becke. [26] Molecular geometries were optimized without constraints. Some counter measures to induce SCF convergence were included, namely level shift (0.15) to induce a HOMO-LUMO gap and strong damping (density mixing step of 0.05). A data set collection of computational results is available in the ioChem-BD repository[27] and can be accessed via http://dx.doi.org/10.19061/iochem-bd-1-22.

Acknowledgements

GA thanks the Generalitat de Catalunya for the prize *ICREA Academia 2008* and *2013* and the ERC for a Starting Grant (258060 FuncMolQIP). The authors thank the Spanish MINECO for funding through CTQ2012-32247, CTQ2015-68370-P (GA, LAB, DA, VV), CTQ2014–52824-R (CB, JGF, NAGB), MAT2014-53961-R (OR), the Marie Curie Co-funding of Regional, National, and International Programmes (COFUND) for funding scheme 291787-ICIQ-IPMP and Fundação para a Ciência e Tecnologia Grant SFRH/BPD/110419/2015 (NAGB) and the Severo Ochoa Excellence Accreditation SEV-2013–0319 (CB). Also we thank Generalitat de Catalunya for financial support through the CERCA Programme and 2014SGR409 grant. The Advanced Light Source is supported by the Director, Office of Science, Office of Basic Energy Sciences of the U. S. Department of Energy under contract no. DE-AC02-05CH11231.

Keywords: Lanthanides • Coordination Chemistry • Supramolecular Chemistry • DFT Calculations • Functional Molecules

[1] a) A. d. Bettencourt-Dias, *Luminescence of Lanthanide Ions in Coordination Compounds and Nanomaterials*, John Wiley & Sons Ltd, Chichester, United Kingdom, **2014**, p. I-XIV; b) R. A. Layfield and M. Murugesu, *Lanthanides and Actinides in Molecular Magnetism*, Wiley-VCH Verlag GmbH & Co. KGaA, Weinheim, Germany, **2015**, p. I-XVIII; c) C. Huang, *Rare Earth Coordination Chemistry*, John Wiley & Sons, Ltd, Singapore, **2010**, p. i-xxiii.
[2] a) Y. M. Li, W. W. Kuang, L. L. Zhu, Y. Xu and P. P. Yang, *European Journal of Inorganic Chemistry* **2016**, *2016*, 4996-5003; b) A. T. Wagner and P. W. Roesky, *European Journal of Inorganic Chemistry* **2016**, *2016*, 782-791; c) P. Zhang, Y. N. Guo and J. K. Tang, *Coordination Chemistry Reviews* **2013**, *257*, 1728-1763.
[3] a) S. Faulkner and M. Tropiano in *Heterometallic Complexes Containing Lanthanides*, *Vol.* John Wiley & Sons Ltd, **2014**, pp. 331-358; b) Y. G. Huang, F. L. Jiang and M. C. Hong, *Coordination Chemistry Reviews* **2009**, *253*, 2814-2834; c) K. Liu, W. Shi and P. Cheng, *Coordination Chemistry Reviews* **2015**, *289*, 74-122.
[4] a) M. Andruh, J. P. Costes, C. Diaz and S. Gao, *Inorganic Chemistry* **2009**, *48*, 3342-3359; b) L. R. Piquer and E. C. Sanudo, *Dalton Transactions* **2015**, *44*, 8771-8780.
[5] a) J.-P. Costes and F. Nicodème, *Chemistry – A European Journal* **2002**, *8*, 3442-3447; b) J.-P. Costes, F. Dahan and F. Nicodème, *Inorganic Chemistry* **2003**, *42*, 6556-6563; c) S. Faulkner and S. J. A. Pope, *Journal of the American Chemical Society* **2003**, *125*, 10526-10527; d) P. Zhu, N. Pan, R. Li, J. Dou, Y. Zhang, D. Y. Y. Cheng, D. Wang, D. K. P. Ng and J. Jiang, *Chemistry – A European Journal* **2005**, *11*, 1425-1432; e) D. J. Lewis, P. B. Glover, M. C. Solomons and Z. Pikramenou, *Journal of the American Chemical Society* **2011**, *133*, 1033-1043; f) R. Sato, K. Suzuki, M. Sugawa and N. Mizuno, *Chemistry – A European Journal* **2013**, *19*, 12982-12990; g) Y. Lan, S. Klyatskaya, M. Ruben, O. Fuhr, W. Wernsdorfer, A. Candini, V. Corradini, A. Lodi Rizzini, U. del Pennino, F. Troiani, L. Joly, D. Klar, H. Wende and M. Affronte, *Journal of Materials Chemistry C* **2015**, *3*, 9794-9801.
[6] a) L. S. Natrajan, A. J. L. Villaraza, A. M. Kenwright and S. Faulkner, *Chemical Communications* **2009**, 6020-6022; b) M. P. Placidi, A. J. L. Villaraza, L. S. Natrajan, D. Sykes, A. M. Kenwright and S. Faulkner, *Journal of the American Chemical Society* **2009**, *131*, 9916-9917; c) J. A. Tilney, T. J. Sorensen, B. P. Burton-Pye and S. Faulkner, *Dalton Transactions* **2011**, *40*, 12063-12066.
[7] M. Seitz, A. G. Oliver and K. N. Raymond, *Journal of the American Chemical Society* **2007**, *129*, 11153-11160.
[8] a) N. André, T. B. Jensen, R. Scopelliti, D. Imbert, M. Elhabiri, G. Hopfgartner, C. Piguet and J.-C. G. Bünzli, *Inorganic Chemistry* **2004**, *43*, 515-529; b) N. Andre, R. Scopelliti, G. Hopfgartner, C. Piguet and J.-C. G. Bunzli, *Chemical Communications* **2002**, 214-215.
[9] S. Floquet, M. Borkovec, G. Bernardinelli, A. Pinto, L.-A. Leuthold, G. Hopfgartner, D. Imbert, J.-C. G. Bünzli and C. Piguet, *Chemistry – A European Journal* **2004**, *10*, 1091-1105.
[10] a) N. Dalla-Favera, J. Hamacek, M. Borkovec, D. Jeannerat, G. Ercolani and C. Piguet, *Inorganic Chemistry* **2007**, *46*, 9312-9322; b) T. Riis-Johannessen, N. Dalla Favera, T. K. Todorova, S. M. Huber, L. Gagliardi and C. Piguet, *Chemistry – A European Journal* **2009**, *15*, 12702-12718.
[11] F. Artizzu, F. Quochi, L. Marchio, R. F. Correia, M. Saba, A. Serpe, A. Mura, M. L. Mercuri, G. Bongiovanni and P. Deplano, *Chemistry-a European Journal* **2015**, *21*, 3882-3885.
[12] J. Zhou, Q. Liu, W. Feng, Y. Sun and F. Y. Li, *Chemical Reviews (Washington, DC, United States)* **2015**, *115*, 395-465.
[13] I. Mamedov, T. N. Parac-Vogt, N. K. Logothetis and G. Angelovski, *Dalton Transactions* **2010**, *39*, 5721-5727.
[14] a) O. Guillou, C. Daiguebonne, G. Calvez and K. Bernot, *Accounts of Chemical Research* **2016**, *49*, 844-856; b) M. S. Tremblay and D. Sames, *Chemical Communications* **2006**, 4116-4118.
[15] G. Aromí, D. Aguilà, P. Gamez, F. Luis and O. Roubeau, *Chemical Society Reviews* **2012**, *41*, 537-546.
[16] a) D. Aguila, L. A. Barrios, V. Velasco, L. Arnedo, N. Aliaga-Alcalde, M. Menelaou, S. J. Teat, O. Roubeau, F. Luis and G. Aromi, *Chemistry-a European Journal* **2013**, *19*, 5881-5891; b) D. Aguila, L. A. Barrios, F. Luis, A. Repolles, O. Roubeau, S. J. Teat and G. Aromi, *Inorganic Chemistry* **2010**, *49*, 6784-6786.
[17] D. Aguilà, L. A. Barrios, V. Velasco, O. Roubeau, A. Repollés, P. J. Alonso, J. Sese, S. J. Teat, F. Luis and G. Aromí, *Journal of the American Chemical Society* **2014**, *136*, 14215-14222.
[18] P. D'Angelo, A. Zitolo, V. Migliorati, G. Chillemi, M. Duvail, P. Vitorge, S. Abadie and R. Spezia, *Inorganic Chemistry* **2011**, *50*, 4572-4579.
[19] a) D. Casanova, J. Cirera, M. Llunell, P. Alemany, D. Avnir and S. Alvarez, *Journal of the American Chemical Society* **2004**, *126*, 1755-1763; b) J. Cirera, E. Ruiz and S. Alvarez, *Chemistry – A European Journal* **2006**, *12*, 3162-3167; c) M. Pinsky and D. Avnir, *Inorganic Chemistry* **1998**, *37*, 5575-5582.
[20] G. M. Sheldrick in *SAINT and SADABS*, *Vol.* Bruker AXS Inc., Madison, Wisconsin, USA, **2012**.
[21] G. M. Sheldrick, *Acta Cryst. A* **2008**, *64*, 112-122.
[22] G. M. Sheldrick, *Acta Cryst. C* **2015**, *71*, 9-18.
[23] A. D. Becke, *Physical Review A* **1988**, *38*, 3098-3100.
[24] a) J. P. Perdew, *Physical Review B* **1986**, *33*, 8822-8824; b) J. P. Perdew, *Physical Review B* **1986**, *34*, 7406-7406.
[25] a) E. Van Lenthe and E. J. Baerends, *Journal of Computational Chemistry* **2003**, *24*, 1142-1156; b) E. Van Lenthe, E. J. Baerends and J. G. Snijders, *The Journal of Chemical Physics* **1993**, *99*, 4597-4610.

[26] A. D. Becke, *The Journal of Chemical Physics* **1988**, *88*, 2547-2553.
[27] M. Álvarez-Moreno, C. de Graaf, N. López, F. Maseras, J. M. Poblet and C. Bo, *Journal of Chemical Information and Modeling* **2015**, *55*, 95-103.

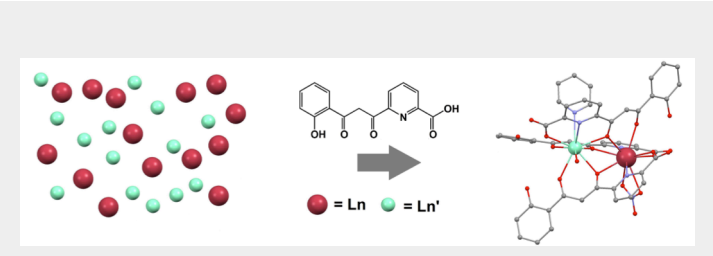

J. Gónzalez-Fabra, N. A. G. Bandeira, V. Velasco, L. A. Barrios, D. Aguilà, S. J. Teat, O. Roubeau, Carles Bo and G. Aromí**

Page No. – Page No.

Thermodynamic Stability of Heterodimetallic [LnLn'] Complexes: Synthesis and DFT Studies